ACS APPLIED MATERIALS & INTERFACES

Research Article

www.acsami.org

Effective Adsorption and Enhanced Removal of Organophosphorus Pesticides from Aqueous Solution by Zr-Based MOFs of UiO-67

Xiangyang Zhu, Bing Li, Jian Yang, Yongsheng Li, Wenru Zhao, Jianlin Shi, and Jinlou Gu*

Key Laboratory for Ultrafine Materials of Ministry of Education, School of Materials Science and Engineering, East China University of Science and Technology, Shanghai 200237, China

Supporting Information

ABSTRACT: Though many efforts have been devoted to the adsorptive removal of hazardous materials of organophosphorus pesticides (OPs), it is still highly desirable to develop novel adsorbents with high adsorption capacities. In the current work, the removal of two representative OPs, glyphosate (GP) and glufosinate (GF), was investigated by the exceptionally stable Zr-based MOFs of UiO-67. The abundant Zr−OH groups, resulting from the missing-linker induced terminal hydroxyl groups and the inherent bridging ones in Zr−O clusters of UiO-67 particles, served as natural anchorages for efficient GP and GF capture in relation with their high affinity toward phosphoric groups in OPs. The correlation between the most significant parameters such as contact time, OPs concentration, adsorbent dose, pH, as well as ionic strength with the adsorption capacities was optimized, and the effects of these parameters on the removal efficiency of GP and GF from the polluted aqueous solution were investigated. The adsorption of GP on UiO-67 was faster than that of GF, and a pseudo-second-order rate equation effectively described the uptake kinetics. The Langmuir model exhibited a better fit to adsorption isotherm than the Freundlich model. Thanks to the strong affinity and adequate pore size, the adsorption capacities in UiO-67 approached as high as 3.18 mmol (537 mg) g^{-1} for GP and 1.98 mmol (360 mg) g^{-1} for GF, which were much higher than those of many other reported adsorbents. The excellent adsorption characteristics of the current adsorbents toward OPs were preserved in a wide pH window and high concentration of the background electrolytes. These prefigured the promising potentials of UiO-67 as novel adsorbent for the efficient removal of OPs from aqueous solution.

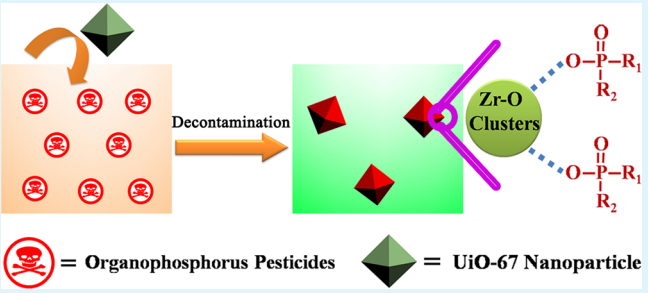

KEYWORDS: *porous adsorbents, metal−organic frameworks, UiO-67, organophosphorus pesticides, decontamination, water treatment*

1. INTRODUCTION

Organophosphorus pesticides (OPs), a group of highly toxic synthetic compounds, are widely used for agriculture production.[1] The acute toxicity of OPs is associated with their ability to bind to acetylcholinesterase (AChE), causing neuromuscular paralysis and organ failure.[2−4] It has become a global necessity to efficiently decontaminate OPs with minimal environmental impact. To date, many strategies have been reported on the efficient elimination of OPs from aqueous solutions such as by electrochemistry,[5−7] adsorption,[8,9] enzymatic biodegradation,[10−12] and photocatalysis.[13−15] Among these, removal of OPs by adsorption techniques is regarded as one of the competitive methods thanks to its simple operation and low cost. Developing new adsorbents with high adsorption capacities is of great significance and a challenge for persistent OPs pollution in the environment.

Over the past several years, porous metal−organic frameworks (MOFs) have been developed as a new class of solid adsorbents.[16−18] In contrast to conventional solid adsorbents such as activated carbon[19−21] and mesoporous silica materials,[22−24] MOFs feature tunable pore sizes, versatile framework compositions and exposed active sites.[25−27] Attributing to these characteristics, MOFs have been found to work effectively to remove hazardous materials, such as organosulfur or organic nitrogen compounds,[28−30] dyes[31,32] and aromatic molecules.[33−36] Nevertheless, no work has been reported to use MOFs in the adsorptive removal of OPs from aqueous solutions until now. For efficient adsorption of OPs, not only adequate porosity/pore size of MOFs but also specific active adsorption sites are required.[37] It has been well documented that zirconium oxide (ZrO_2) nanoparticles could selectively capture OPs due to the strong complexing ability of the Zr−OH groups on their surface for the phosphoric groups.[38] Therefore, integrating Zr−OH groups into MOFs could be employed to serve as anchorages for OPs removal. Very recently, we have explored the ultrahigh drug loading capacity of UiO-66 MOFs for bisphosphonates thanks to the abundant Zr−OH groups therein and their large surface area.[39] These hydroxyl groups in Zr-based MOFs originate from the bridging μ_3−OH groups in Zr−O clusters and missing-linker induced

Received: August 31, 2014
Accepted: December 16, 2014
Published: December 16, 2014

DOI: 10.1021/am5059074
ACS Appl. Mater. Interfaces 2015, 7, 223−231

terminal ones, and the latter is more reactive than the bridging hydroxyl groups as reported.[40] On the basis of the high affinity of Zr−OH groups toward phosphoric groups, we further propose an idea that the MOFs with a large amount of Zr−OH groups might be potentially applied for effective removal of OPs.

Glyphosate (GP, N-phosphonomethyl glycine) and glufosinate (GF, DL-homoalanin-4-(methyl) phosphonic acid, see Scheme 1 for their chemical structures), two kinds of OPs, are

Scheme 1. Chemical Structures of (a) Glyphosate and (b) Glufosinate

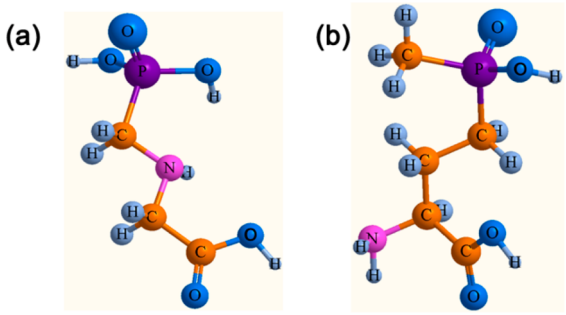

frequently used in agriculture.[41,42] Because of the indiscriminate use, GP and GF have been detected in surface and subsurface water and become large concerns.[43] Owing to their considerable water solubility, they enter the aquatic environment widely and cause harm to human health. In the current work, we report the remarkably enhanced adsorption capacity of these two representative OPs over zirconium-based MOFs of UiO-67, which recently receive great attentions due to their exceptional stability. UiO-67 is composed of linear 4,4′-biphenyldicarboxylic acid (BPDC) ligands and $Zr_6O_4(OH)_4$ clusters as 12-connected nodes.[44] It possesses a face-centered-cubic arrangement of the Zr_6 clusters and consists of octahedral (16 Å) and tetrahedral (12 Å) cages which are larger than the counterpart cages in UiO-66, and consequently more suitable for large molecules of OPs occupation.[45−48] By taking advantages of the open cavities and abundant Zr−OH groups in UiO-67, the adsorption capacities approach 3.18 mmol (537 mg) g^{-1} for GP and 1.98 mmol (360 mg) g^{-1} for GF in the prepared adsorbent, respectively. These values are much higher than those of many other reported adsorbents, prefiguring the great potentials of the current developed adsorbents in environmental pollution management.

2. EXPERIMENTAL DETAILS

2.1. Synthesis of UiO-67. The UiO-67 were prepared according to the literature with slight modification.[44] Briefly, $ZrCl_4$ (233 mg, 1 mmol), 4,4′-biphenyldicarboxylic acid (BPDC, 242 mg, 1 mmol), acetic acid (0.6 g, 10 mmol) and HCl (37%, 12 M; 0.16 mL, 2 mmol) were dissolved in 30 mL of DMF by sonication. The mixture was heated to 120 °C for 48 h. After that, the white product of UiO-67 was harvested by centrifugation and washed three times with DMF. The as-synthesized UiO-67 was soaked in DMF at room temperature for 6 h to remove the free BPDC. Then, the obtained particles were washed with acetone repeatedly to exchange the trapped DMF before drying at 100 °C under vacuum for 24 h.

2.2. Characterization. Powder X-ray diffraction (XRD) patterns were acquired at a rate of 6° min^{-1} over the range of 4−40° (2θ) on Bruker D8 equipped with Cu Kα radiation (40 kV, 40 mA). N_2 adsorption−desorption isotherms were collected with a Quantachrome NOVA 4200E porosimeter at −196 °C. All the samples were degassed under vacuum for 12 h before measurements. The specific surface area and micropore volume were calculated by the Brunauer−Emmett−Teller (BET) method using adsorption data at a relative pressure lower than 0.15. FT-IR spectra were taken with a resolution of 4 cm^{-1} using the KBr method on a Nicolet 7000-C spectroscopy. TEM images were taken on a JEOL JEM-2100 microscope operating at 200 kV. Thermogravimetric analysis (TGA) was conducted on a PerkinElmer thermogravimetric analyzer by heating the sample to 800 °C under air atmosphere (50 mL min^{-1}) at a heating rate of 10 °C min^{-1}. Zeta potentials of the UiO-67 particles at different pHs were measured by the Zetasizer (Nano-ZS) from Malvern Instruments and its software. The UiO-67 was dispersed in water, and the pH value of the solution was adjusted by adding negligible volumes of 0.1 M HCl or 0.1 M NaOH aqueous solutions.

2.3. Adsorption Experiments. An aqueous stock solution of GP or GF (200 ppm) was prepared by dissolving GP ($C_3H_8NO_5P$, MW: 169.07) or GF ($C_5H_{12}NO_4P$, MW: 181.1) in deionized water. GP or GF solutions with different concentrations (0.03−0.4 mmol L^{-1}) were prepared by the dilution of the stock solution with water. The GP or GF concentrations were determined by measuring the phosphorus using ICP-AES. Before adsorption, the UiO-67 were dried at 120 °C in vacuum oven overnight and kept in a desiccator.

The adsorption kinetic studies were conducted at pH 4 with an initial OPs concentration of 0.1 mmol L^{-1} at 25 °C, and the mass ratio of adsorbent to water was kept at 0.03:1000. The residual OPs in a series of independent samples were measured at the time range from 10 min to 10 h. The OPs solutions and the adsorbents were mixed thoroughly at a speed of 160 rpm on a platform shaker. After adsorption for a predetermined time, the mixture was centrifuged and the GP or GF concentrations in the supernatants were determined by measuring the phosphorus using ICP-AES. Batch adsorption experiments of OPs onto UiO-67 were performed in 50 mL of aqueous OPs solutions with different adsorbents concentrations (0.03, 0.05, and 0.1 g L^{-1}) at pH 4 for 5 h. The amounts of adsorbed GP or GF were measured from the difference between the initial (C_0) and equilibrium (C_e) concentrations in the supernatant after centrifugation. The equilibrium uptake was calculated by eq 1

$$q_e = (C_0 - C_e)\frac{V}{W} \quad (1)$$

Where q_e (mmol g^{-1}) is equilibrium adsorption capacity of GP or GF on UiO-67. V presents the volume of the used OPs solution (L), and W is the weight of the used adsorbents (g).

To estimate the adsorption capacities at different pHs, we adjusted the pH of the OPs solutions by adding negligible volumes of 0.1 M HCl or 0.1 M NaOH aqueous solutions. To study the interference effect of the other ions on the OPs adsorption onto the UiO-67 adsorbents, various salt solutions including $CaCl_2$, NaOAc, $MgSO_4$, and KNO_3 with different concentrations were added into the adsorption solutions under otherwise the same condition as the above adsorption experiments.

2.4. Data Analysis. The adsorption kinetics of UiO-67 were analyzed by pseudo-first-order, pseudo-second-order kinetic models and intraparticle diffusion kinetic model. The Langmuir adsorption and Freundlich adsorption models were used to fit the adsorption isotherms for GP and GF.

3. RESULTS AND DISCUSSION

3.1. Characterization of UiO-67. The highly crystallized UiO-67 were prepared by a modified solvothermal method.[44] As confirmed by powder XRD pattern (Figure 1a), the synthesized materials exhibit the characteristic cubic close packed structure in consistence with the reported work.[49] TEM image reveals that the discrete particle of UiO-67 is in irregular shape, and the particle size is in submicrometer scale (Figure S1, Supporting Information). The textural properties of the synthesized UiO-67 were examined by nitrogen sorption technique. The adsorption−desorption curve presents the

DOI: 10.1021/am5059074
ACS Appl. Mater. Interfaces 2015, 7, 223−231

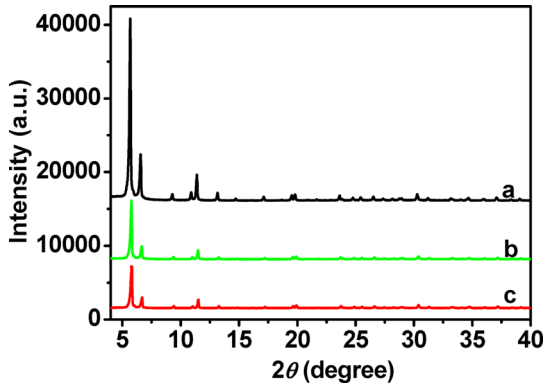

Figure 1. XRD patterns of (a) the as-synthesized UiO-67, (b) GF adsorbed UiO-67, and (c) GP adsorbed UiO-67.

characteristic steps and type IV isotherm in agreement with the previous observation for UiO-67 structures (Figure 2a).[46] The

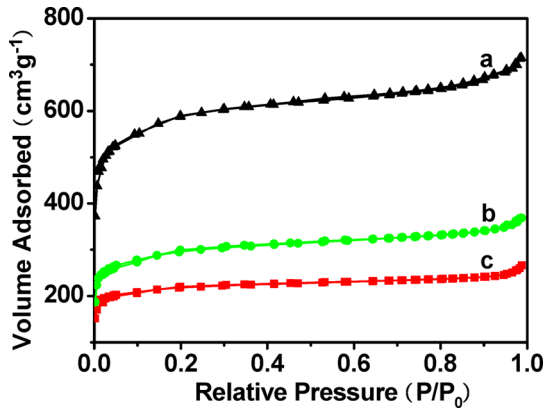

Figure 2. Nitrogen adsorption–desorption isotherms of (a) UiO-67, (b) GF adsorbed UiO-67, and (c) GP adsorbed UiO-67.

Brunauer–Emmett–Teller (BET) surface area is calculated to be 2172 $m^2\ g^{-1}$ by using adsorption data in a relative pressure range from 0.05 to 0.15, which is similar to the value reported (2300 $m^2\ g^{-1}$).[49] Pore sizes are determined to be 1.17 and 1.61 nm by the DFT method (Figure S2, Supporting Information), which correspond to the tetrahedral and octahedral pores in UiO-67, respectively.[46] Trace amount of mesopore (ca. 2.3 nm) is also present as Figure S2 illustrated, implying UiO-67 might be defective resulting from the linker missing.[48] The TGA data show that UiO-67 is stable in air up to 500 °C (Figure S3, Supporting Information). Dehydroxylation of $Zr_6O_4(OH)_4$ clusters is completed at 300 °C, and the unit becomes $Zr_6O_6(BPDC)_6$ in theory.[44,46] When temperature reaches 650 °C, only ZrO_2 leaves. Based on the values of weight (%) at 300 and 650 °C (94.1% and 36%, respectively), the number of BPDC in each unit is calculated to be 5.4, confirming the presence of defects originated from the linker missing in the obtained UiO-67 in agreement with the N_2 sorption analysis.[45,46]

3.2. Adsorptive Kinetics. The adsorptions of GP and GF from aqueous solution onto UiO-67 as a function of contact time are shown in Figure 3a. The adsorption capacities for both OPs increase rapidly during the first 60 min and reach adsorption equilibrium in approximate 150 min for GP and 200 min for GF, respectively. The rapid removal rate of pollutants at the initial period could be ascribed to the fact that abundant of vacant adsorption sites are available initially. After a lapse of time, the concentration of available sites becomes lower, resulting in gradually decreased adsorption rate at higher conversion. Besides, the cavities in the adsorbents might be partially blocked by the captured OPs molecules, which maybe also has a negative impact on the adsorption rate. Based on these results, 300 min was selected as the shaking time to ensure the full equilibrium in the following experiments. The changes of adsorbed amount with time were simulated with a pseudo-first-order model (Figure 3b) and a pseudo-second-order model (Figure 3c), respectively. The pseudo-second-order eqs 2 and 3 are generally expressed as

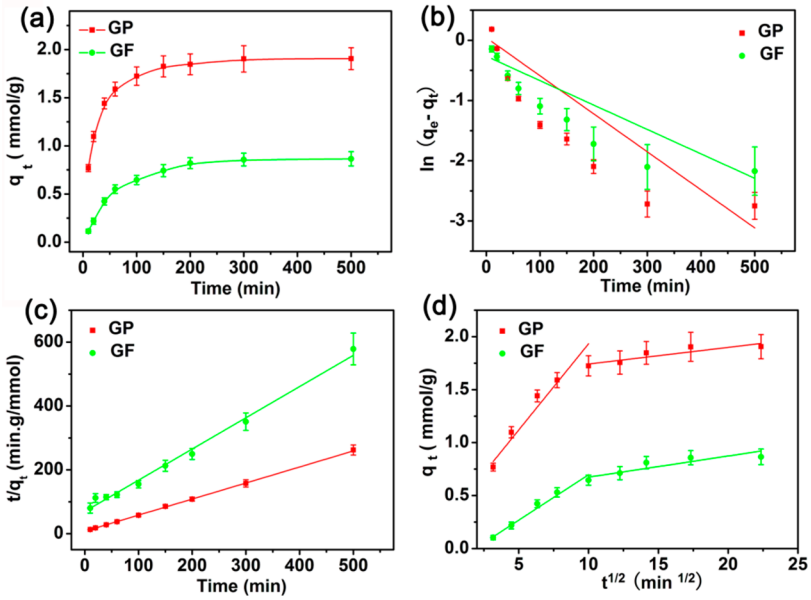

Figure 3. (a) Effect of contact time on the GP (red) and GF (green) adsorption over UiO-67, and the corresponding plots of (b) pseudo-first-order kinetics, (c) pseudo-second-order kinetics, and (d) intraparticle diffusion kinetics of OPs adsorption (25 °C, pH 4, $C_{initial}$ = 0.1 mmol L^{-1}).

DOI: 10.1021/am5059074
ACS Appl. Mater. Interfaces 2015, 7, 223–231

Table 1. Kinetic Parameters of Pseudo-First-Order, Pseudo-Second-Order, and Weber–Morris Models for GP and GF on UiO-67 ($C_{initial}$ = 0.1 mmol L^{-1}, UiO-67 = 0.03 g L^{-1}, T = 25 °C, pH 4)

	pseudo-first-order model			pseudo-second-order model			intraparticle diffusion model		
OPs	k_1 (min^{-1})	q_e (mmol g^{-1})	R^2	k_2 (min^{-1})	q_e (mmol g^{-1})	R^2	k_i	I (mmol g^{-1})	R^2
GP	0.0135 ± 0.0028	0.64 ± 0.13	0.669	0.0342 ± 0.0005	1.97 ± 0.014	0.999	0.0156 ± 0.0041	1.590 ± 0.062	0.935
GF	0.0098 ± 0.0011	0.62 ± 0.07	0.705	0.0152 ± 0.0011	0.98 ± 0.042	0.992	0.0178 ± 0.0055	0.511 ± 0.081	0.951

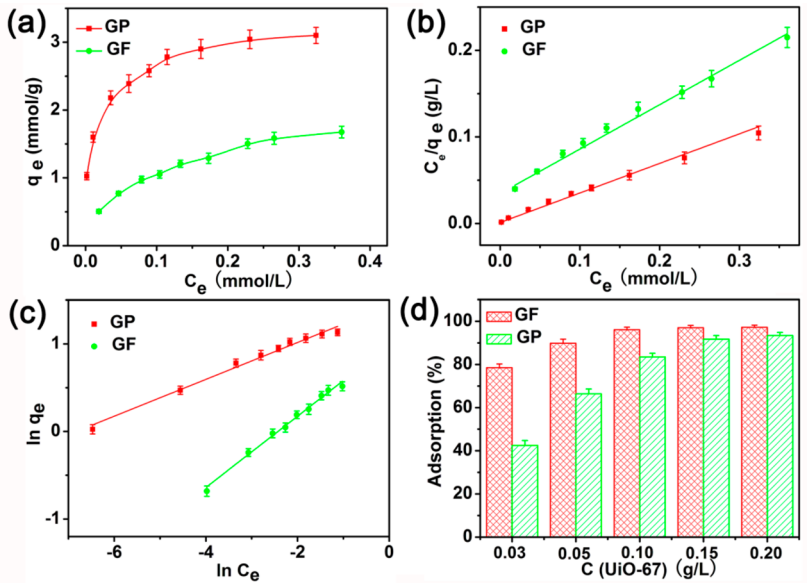

Figure 4. (a) Isotherms for the adsorption of GP (red) and GF (green) on UiO-67; the corresponding plots of (b) Langmuir model and (c) Freundlich model of OPs adsorption (25 °C, pH 4, $C_{adsorbent}$ = 0.03 g L^{-1}); (d) Effect of UiO-67 content on the adsorption of GP and GF (25 °C, pH 4, $C_{initial}$ = 0.05 mmol L^{-1}).

$$\frac{dq}{dt} = k_2(q_e - q_t)^2 \tag{2}$$

or

$$\frac{t}{q_t} = \frac{1}{k_2 q_e^{\,2}} + \frac{t}{q_e} \tag{3}$$

where q_e (mmol g^{-1}) and q_t (mmol g^{-1}) are the amounts of GP or GF adsorbed at equilibrium and at time t (min), respectively; t (min) is adsorption time, and k_2 (g $mmol^{-1}$ min^{-1}) is the pseudo-second-order adsorption rate constant. k_2 can be calculated from the slope and intercept of plot t/q_t versus t.

The kinetic parameters and correlation coefficients are listed in Table 1. In comparison with the pseudo-first-order kinetic model, the pseudo-second-order kinetic model fits the experimental data better with correlation coefficients (R^2) higher than 0.99. Moreover, the equilibrium adsorption amounts (q_e) calculated from fitting results approach the experimental data for GP and GF (1.90 and 0.87 mmol g^{-1}, respectively). These results suggest that both GP and GF adsorptions on UiO-67 follow the pseudo-second-order model, which was developed based on the assumption that limiting step may be a chemisorptions process involving valency forces via sharing (or exchange) of electrons between adsorbate and adsorbent.[50,51]

Furthermore, the kinetic parameter of k_2 for GF is much less than that for GP, indicating the affinity of UiO-67 is weaker toward GF compared to GP.[43] This could be probably attributed to the replacement of hydroxyl by methyl (see Scheme 1), which alters the electronics at phosphorus and decreases the number of hydroxyl groups on phosphorus, thereby weakens the adsorbents-OPs interactions.

To further understand the adsorption kinetics, intraparticle diffusion kinetics model was tested to elucidate the diffusion mechanism (Figure 3d). According to Weber and Morris, the intraparticle diffusion eq 4 could be expressed as

$$q_t = k_i t^{0.5} + I \tag{4}$$

where k_i (mmol g^{-1} $min^{-0.5}$) is the intraparticle diffusion rate constant; I is the intercept, and the corresponding kinetic parameters are given in Table 1. Plots of q_t vs $t^{0.5}$ can be divided into two linear segments, indicating that diffusion process proceeds via two steps. The initial portion represents boundary layer diffusion ascribed to the external mass transfer of OPs from bulk solution to the outer surface of adsorbents. The second phase is controlled by intraparticle diffusion of OPs throughout the open cavities of the UiO-67.[43,52] In addition, the plots do not pass through the origin, demonstrating that the intraparticle diffusion is not the sole rate-controlling step.[53] The slope of the second linear portion of the plot has been defined as the intraparticle diffusion parameter k_i (mmol g^{-1} $min^{-0.5}$). The proximity of the both k_i values (see Table 1) for GP and GF implies the almost identical diffusion rates of both OPs in the cages of the UiO-67 adsorbents. The intercept of the plot reflects the effect of the boundary layer, and the larger intercept corresponds to the greater contribution of the boundary layer effect on the rate-controlling step.[52] Thus, the presence of multilinearity indicates that the external mass transfer may also play a significant role in the OPs adsorption process. Therefore,

DOI: 10.1021/am5059074
ACS Appl. Mater. Interfaces 2015, 7, 223–231

Table 2. Langmuir and Freundlich Parameters of UiO-67 for GP and GF Adsorption

		Langmuir model			Freundlich model		
OPs	UiO-67 dose (g L^{-1})	k_L (L $mmol^{-1}$)	q_{max} (mmol g^{-1})	R^2	k_F ($mmol^{1-n}$ L^n g^{-1})	n	R^2
GP	0.03	78.70 ± 18.47	3.18 ± 0.15	0.995	4.40 ± 0.13	0.222 ± 0.010	0.988
	0.05	150.62 ± 57.83	2.74 ± 0.13	0.994	4.01 ± 0.19	0.206 ± 0.014	0.975
	0.1	137.62 ± 23.02	2.25 ± 0.06	0.998	3.78 ± 0.39	0.230 ± 0.031	0.905
GF	0.03	13.42 ± 0.96	1.98 ± 0.06	0.991	2.70 ± 0.09	0.412 ± 0.014	0.985
	0.05	14.10 ± 0.85	1.71 ± 0.06	0.993	2.58 ± 0.14	0.397 ± 0.033	0.961
	0.01	19.36 ± 0.79	1.13 ± 0.02	0.997	2.01 ± 0.17	0.454 ± 0.042	0.949

the adsorptive removal of GP and GF could be cooperatively controlled by external mass transfer and intraparticle diffusion.

3.3. Adsorption Isotherms for GP and GF Removal. The adsorption isotherms of GP and GF on UiO-67 were assessed at 25 °C after their adsorption for a sufficient period of 300 min (Figure 4a). Two most commonly used isotherm models, Langmuir and Freundlich models, were employed to simulate the adsorption isotherms (Figure 4b, c). The linear mathematical expression 5 of the Langmuir model is presented as

$$\frac{C_e}{q_e} = \frac{1}{k_L q_{max}} + \frac{C_e}{q_{max}} \quad (5)$$

where C_e is the equilibrium concentration of OPs (mmol L^{-1}), q_e is the amount of adsorbed OPs at equilibrium (mmol g^{-1}), k_L represents the Langmuir constant (L $mmol^{-1}$) that relates to the adsorption energy and affinity of binding sites, and q_{max} denotes the maximum adsorption capacity (mmol g^{-1}).

Freundlich adsorption eq 6 has the linear form as following

$$\log q_e = \log k_F + (n)\log C_e \quad (6)$$

where k_F ($mmol^{1-n}$ L^n g^{-1}) is the Freundlich constant related to the adsorption capacity of the adsorbent, and n signifies adsorption intensity.[53] The value of n reflects the type of isotherm to be favorable ($0 < n < 1$), irreversible ($n = 0$) or unfavorable ($n > 1$).

The related parameters and correlation coefficients (R^2) of the two models are tabulated in Table 2. From R^2 and fitting lines, it can be found that the Langmuir model exhibits better fit than the Freundlich model. The more appropriate fit of Langmuir isotherm could be ascribed to the homogeneous distribution of active adsorption sites on the surface of UiO-67, as the Langmuir equation assumes that the surface of adsorbent is homogeneous. The uptake capacities of OPs decrease with increasing adsorbent dose (see Figure S4 in the Supporting Information), implying that the adsorption is a diffusion-driven process, including the bulk phase to the surface of the adsorbent and intraparticle diffusion.[54] The maximum adsorption capacities of GP and GF by UiO-67 are calculated to be 3.18 mmol (537 mg) g^{-1} and 1.98 mmol (360 mg) g^{-1}, respectively. The q_{max} of GP is larger than that of GF, demonstrating that the UiO-67 present different affinities to OPs with different molecular structures. The presence of methyl on the phosphorus atom of the GF might diminish its bonding with the Zr−OH groups in UiO-67, and these results correlate well with the adsorptive kinetic analysis. It should be pointed out that adsorption capacities of GP and GF on UiO-67 are much higher than those of many other reported adsorbents. A comparison of the adsorption capacities of GP by various materials is shown in Table 3, which reveals the great advantage of our strategy by employing UiO-67 as potential adsorbents for OPs cleanup.

Table 3. Comparison of the Adsorption Capacities of GP onto Various Adsorbents

adsorbents	q_{max} (mg g^{-1})	ref
UiO-67	537	this work
MgAl−LDH	184.6	9
Ni_2AlNO_3−LDH	172.4	43
α-FeOOH	38.0	55
Montmorillonite	49.9	56
Alum sludge	85.9−113.6	57
Polyaniline/ZSM-5	8.9−98.5	58

The influence of adsorbent content on the adsorptive removal of GP and GF was further investigated (Figure 4d). As expected, the adsorption percentages of GP and GF increase with the increase of UiO-67 dose in the suspension. More than 96% of GP is removed at 0.1 g L^{-1} adsorbent dosage, whereas about 91.7% of GF is adsorbed at 0.15 g L^{-1} UiO-67 dosage. Given the high removal efficiency for GP and GF with the low applied level of UiO-67, we do believe that the UiO-67 can be promising adsorbents for the effective removal of OPs from the contaminated aqueous solution.

3.4. Effects of pH and Ionic Strength. The effect of pH on the adsorption of GP and GF onto UiO-67 was estimated in the pH range from 2 to 9 (Figure 5a). The GP molecules exhibit the aqueous dissociation constants as $pK_1 < 2$, $pK_2 = 2.6$, $pK_3 = 5.6$, $pK_4 = 10.6$ and those of GF are $pK_1 = 2$, $pK_2 = 2.9$, $pK_3 = 9.8$.[43] Hence, in most of the experimental pH range, these two adsorbates are negatively charged. Moreover, we measured the zeta potential of the adsorbent, and found that the surface charge of UiO-67 remained negative above pH 2 (Figure S5, Supporting Information). Thus, the electrostatic attraction between the negatively charged adsorbent and GP (or GF) could be neglected. This indicates that the uptake of GP and GF onto the UiO-67 could be chemisorption rather than electrostatic adsorption.[59] It is found that UiO-67 adsorbents work effectively over a wide range of pH, and the maximum OPs removal is observed at pH 4 for GP and at pH 5 for GF. The uptakes of GP and GF decrease at higher pH (>7), which may be due to the fact that electrostatic repulsion between the electronegative OPs and the negatively charged sorbent became strong.

As there are various salts and metal ions in environmental water, the effect of ionic strength on the adsorption capacities of GP (Figure 5b) and GF (Figure S6, Supporting Information) onto UiO-67 was also studied. Different concentrations (5 and 50 mM) of $CaCl_2$, NaOAc, $MgSO_4$ and KNO_3 were utilized in current investigation. Only slight changes of the adsorption capacities are observed when adding different concentrations of

DOI: 10.1021/am5059074
ACS Appl. Mater. Interfaces 2015, 7, 223−231

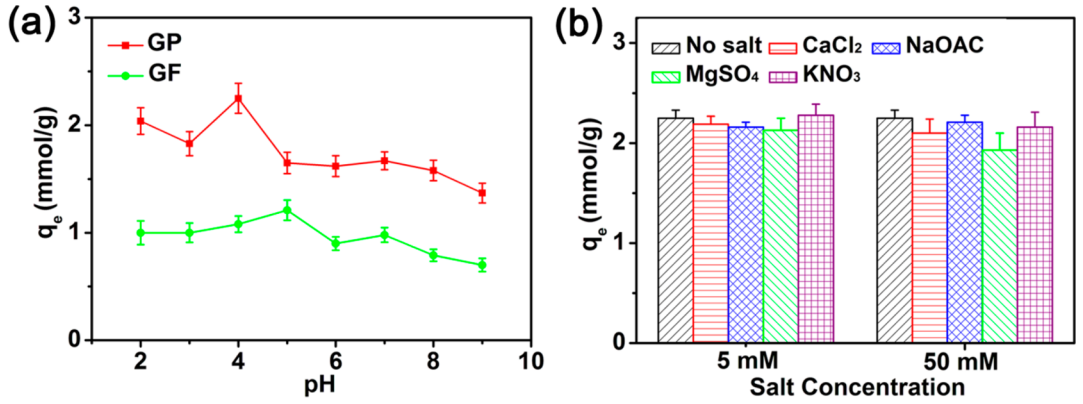

Figure 5. (a) Effect of pH values on the adsorption of GP (red) and GF (green) onto UiO-67 (25 °C, $C_{initial}$ = 0.16 mmol L^{-1}). (b) Effect of ionic strength on the adsorption of GP onto UiO-67 (25 °C, pH 4, $C_{initial}$ = 0.16 mmol L^{-1}).

the electrolytes. This elucidates that metallic ions have negligible effect on the binding affinity between the adsorbents and the adsorbed species. The background salts could affect the binding of the adsorbing species by influencing the thickness and interface potential of the double layer (the interface of adsorbents and the background solution).[60] Generally, the adsorption can be classified into outer-sphere complexes (weakly bonding) and inner-sphere complexes (strongly bonding).[60] Because the outer-sphere complexes and electrolyte ions are placed in the same plane (β-plane), outer-sphere complexes of adsorbates are expected to be more sensitive to the changes in ionic strength than inner-sphere complexes.[60,61] Therefore, the adsorption of OPs probably takes place through the formation of inner-sphere surface complexes.

3.5. Other Physicochemical Determinations. We employed XRD technique to characterize the structural evolvement of the synthesized UiO-67 and OPs adsorbed UiO-67 (GP-UiO-67 and GF-UiO-67, respectively). All the samples exhibit the similar Bragg diffraction peaks, indicating that the OPs adsorption did not change the parent crystalline structure of UiO-67 (Figure 1b, c). However, for OPs adsorbed UiO-67, the relative intensities of all the peaks are weakened as compared to that of the parent UiO-67, which might be ascribed to the trapping of the OPs in the UiO-67 cavities and consequently leads to the diminished X-ray contrast between porous framework and pore cages.[62] The nitrogen adsorption–desorption curves for both of GP-UiO-67 and GF-UiO-67 display typical IV isotherms (Figure 2b, c). This further affirms the fact that the OPs treatment did not destroy the structure integrity of UiO-67. As expected for the OPs molecules occupation in the cages of adsorbents, the dramatic decreases in the surface area and pore volume are observed for OPs adsorbed UiO-67 (Table 4).

Fourier transformed infrared (FT-IR) spectra were collected to shed light on the molecular interaction of OPs with UiO-67 adsorbents. For pristine UiO-67 (Figure 6A), the triplet at 769, 710, and 660 cm^{-1} (labeled with green arrows) are assigned to Zr–O_2 as longitudinal and transverse modes, respectively.[44] The intense doublet at 1600 and 1420 cm^{-1} (labeled with purple stars) can be ascribed to the in- and out-of-phases stretching modes of the carboxylate groups.[44] After GP loading, the broad P–O stretching bands between 1200 and 900 cm^{-1} containing three main characteristic absorption bands and a shoulder appear in the spectrum (Figure 6Ac), confirming the adsorption of GP by UiO-67. The bands at 1164, 1100, 1028 cm^{-1} correspond to the P═O, antisymmetric and symmetric vibrations of P–O bands, respectively, and the shoulder at 935 cm^{-1} might probably be assigned to P–O–Zr bond.[63,64] In the spectrum of GF-UiO-67 (Figure S7, Supporting Information), new peaks at 1100 and 1031 cm^{-1}, ascribing to antisymmetric and symmetric vibrations of P–O, also verify that the OPs of GF have been effectively adsorbed by the highly efficient adsorbents of UiO-67. We note that the P–O bands in the GP and GF molecule (labeled with pink arrows in Figure 6A and Figure S7 in the Supporting Information) have been substantially red-shifted, which is plausible because binding of OP molecules to the Zr–OH groups in UiO-67 could significantly decrease the frequency of the P–O stretching modes.[64]

We also measured the XPS spectra of O, Zr and P of OPs adsorbed UiO-67 to further provide the information on the interaction between UiO-67 and adsorbates (Figure S8, Supporting Information). Compared with the O 1s spectra of the parent UiO-67 (Figure S9, Supporting Information), those of OPs adsorbed UiO-67 are significantly different. For GP-UiO-67, the deconvoluted O 1s spectrum (Figure 6B) consists of four peaks, which could be assigned to O in O–C═O (533.6 eV), P–O–H (532.6 eV), Zr–O–Zr (530.6 eV), and in Zr–O–P and P═O (531.7 eV), respectively.[65] Similar peaks can be observed in the deconvoluted O 1s peak of GF-UiO-67 (Figure S10, Supporting Information). These strongly verify that the Zr–OH groups in UiO-67 present high affinity toward GP and GF molecules, and also rationalize that the chemisorption could probably be involved in the OPs adsorption process in agreement with the kinetic analysis.

According to the FT-IR and XPS analysis, the following adsorption mechanism may be deduced. The missing-linker defects exist in the resultant UiO-67 as TGA illustrated, which would make the OH^- complete the Zr-coordination sphere.[48,66] These missing-linker-induced Zr–OH groups are very reactive as reported,[40,66] which could effectively complex with OPs and form the Zr–O–P bonds to facilitate the OPs sequestration. This is probably one of the main reasons for the

Table 4. Textural Parameters of UiO-67, GF-UiO-67, and GP-UiO-67

samples	S_{BET} (m^2 g^{-1})	V_P (cm^3 g^{-1})
UiO-67	2172	1.12
GF-UiO-66	925	0.64
GP-UiO-67	538	0.41

DOI: 10.1021/am5059074
ACS Appl. Mater. Interfaces 2015, 7, 223–231

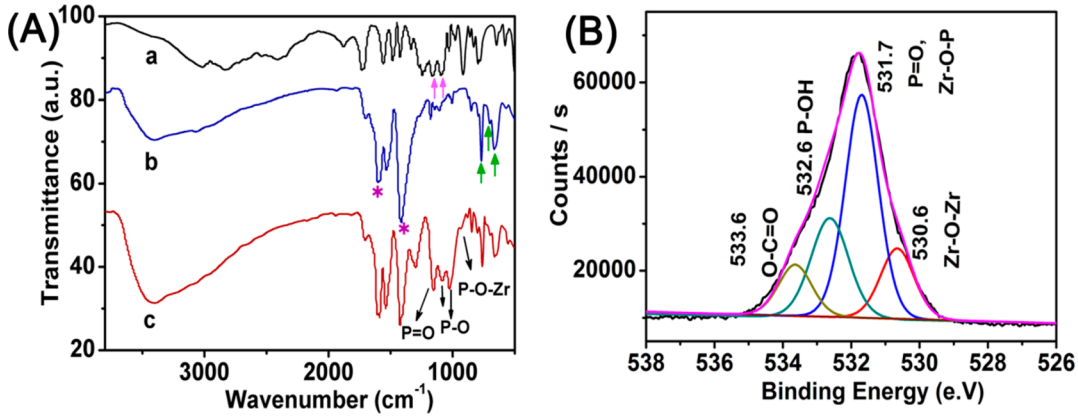

Figure 6. (A) FT-IR spectra of (a) GP molecule, (b) parent UiO-67, and (c) GP adsorbed UiO-67. (B) O 1s XPS spectrum of GP-UiO-67.

enhancement of the OPs adsorption. Besides, we cannot rule out the other factors that might be involved. The inherent bridging Zr−OH of $Zr_6O_4(OH)_4$ clusters might also serve as the natural anchorages to complex the P−O bonds in GP and GF molecules.[39,40,67] It was verified by a titration method[68] that the amount of these bridging hydroxyl groups was identical to the nominal content based on the molecular formula of $Zr_6O_4(OH)_4$ clusters. Because UiO-67 is composed of linear BPDC ligands and $Zr_6O_4(OH)_4$ clusters as connected nodes, large amount of the bridging μ_3−OH in Zr_6 clusters should be present in the framework of MOFs. Additionally, we cannot exclude the possibility that some OPs were captured at the expense of carboxylic groups in BPDC linkers. Given that the structure integrity of the adsorbent was maintained as elucidated by XRD and N_2 sorption techniques, this interaction might be very limited in that the excessive replacement of the bicipital BPDC by monofunctional OPs would deteriorate or even destroy the structure of UiO-67.[46] This is also coincident with the fact that the adsorption experiments were conducted under very mild conditions, e.g. at room temperature with a very short time of 5 h. Taken together, all the above-mentioned mechanisms might result in the formation of the P−O−Zr bonds and rationalize the effective decontamination of OPs with enhanced adsorption capacities using the current adsorbents of UiO-67.

4. CONCLUSIONS

In conclusion, Zr-based MOFs of UiO-67 have been successfully developed as novel adsorbents for the efficient removal of OPs from aqueous solution. The adsorption capacities in the current adsorbents approach as high as 3.18 mmol (537 mg) g^{-1} for GP and 1.98 mmol (360 mg) g^{-1} for GF, respectively. Their outstanding adsorption characteristics toward OPs are preserved in a wide pH window and high concentration of the background salts. The merits of the applied adsorbents, including the abundant active OPs anchorages, high specific surface area as well as the adequate pore size, lead to the remarkably enhanced OPs adsorption capacities. Except the current investigated typical OPs of GL and GF, the newly explored absorbents of UiO-67 could be hopefully expanded for the removal of a wide range of OPs and applied as solid-phase extraction materials for wastewater treatment. Meanwhile, their strong affinity to OPs makes them favorable candidates as chromatographic column materials for the improved retention of these pesticides, consequently enhancing their sensitivity for OPs analysis.

■ ASSOCIATED CONTENT

Supporting Information

TEM image, TGA data, adsorption isotherm of GP and GF with different adsorbent doses, Zeta potential of UiO-67, effect of ionic strength on the adsorption of GF on UiO-67, FT-IR spectra, wide scan XPS spectra and O 1s XPS spectra of parent UiO-67 and GF-UiO-67. This material is available free of charge via the Internet at http://pubs.acs.org.

■ AUTHOR INFORMATION

Corresponding Author

*E-mail: jinlougu@ecust.edu.cn. Fax: +86-21-64250740. Tel: +86-21-64252599.

Notes

The authors declare no competing financial interest.

■ ACKNOWLEDGMENTS

This work was financially supported by the Natural Science Foundation of China (51072053, 51372084, 51132009), the Innovation Program of Shanghai Municipal Education Commission (13zz040), the Nano-Special Foundation for Shanghai Committee of Science and Technology (12 nm0502600), and the 111 Project (B14018).

■ REFERENCES

(1) Lartiges, S. B.; Garrigues, P. P. Degradation Kinetics of Organophosphorus and Organonitrogen Pesticides in Different Waters under Various Environmental Conditions. *Environ. Sci. Technol.* **1995**, *29*, 1246−1254.

(2) Acero, J. L.; Benítez, F. J.; Real, F. J.; González, M. Chlorination of Organophosphorus Pesticides in Natural Waters. *J. Hazard. Mater.* **2008**, *153*, 320−328.

(3) Chanda, A.; Khetan, S. K.; Banerjee, D.; Ghosh, A.; Collins, T. J. Total Degradation of Fenitrothion and Other Organophosphorus Pesticides by Catalytic Oxidation Employing Fe-TAML Peroxide Activators. *J. Am. Chem. Soc.* **2006**, *128*, 12058−12059.

(4) Legierse, K. C. H. M.; Verhaar, H. J. M.; Vaes, W. H. J.; De Bruijn, J. H. M.; Hermens, J. L. M. Analysis of the Time-Dependent Acute Aquatic Toxicity of Organophosphorus Pesticides: The Critical Target Occupation Model. *Environ. Sci. Technol.* **1999**, *33*, 917−925.

(5) Samet, Y.; Agengui, L.; Abdelhédi, R. Electrochemical Degradation of Chlorpyrifos Pesticide in Aqueous Solutions by Anodic Oxidation at Boron-Doped Diamond Electrodes. *Chem. Eng. J.* **2010**, *161*, 167−172.

(6) Arapoglou, D.; Vlyssides, A.; Israilides, C.; Zorpas, A.; Karlis, P. Detoxification of Methyl-Parathion Pesticide in Aqueous Solutions by Electrochemical Oxidation. *J. Hazard. Mater.* **2003**, *98*, 191−199.

DOI: 10.1021/am5059074
ACS Appl. Mater. Interfaces 2015, 7, 223−231

(7) Martínez-Huitle, C. A.; De Battisti, A.; Ferro, S.; Reyna, S.; Cerro-López, M.; Quiro, M. A. Removal of the Pesticide Methamidophos from Aqueous Solutions by Electrooxidation Using Pb/PbO_2, Ti/SnO_2, and Si/BDD Electrodes. *Environ. Sci. Technol.* **2008**, *42*, 6929−6935.
(8) Johnson, B. J.; Malanoski, A. P.; Leska, I. A.; Melde, B. J.; Taft, J. R.; Dinderman, M. A.; Deschamps, J. R. Adsorption of Organophosphates from Solution by Porous Organosilicates: Capillary Phase-Separation. *Microporous Mesoporous Mater.* **2014**, *195*, 154−160.
(9) Li, F.; Wang, Y.; Yang, Q.; Evans, D. G.; Forano, C.; Duan, X. Study on Adsorption of Glyphosate (N-Phosphonomethyl Glycine) Pesticide on MgAl-Layered Double Hydroxides in Aqueous Solution. *J. Hazard. Mater.* **2005**, *125*, 89−95.
(10) Cycoń, M.; Żmijowska, A.; Wójcik, M.; Piotrowska-Seget, Z. Biodegradation and Bioremediation Potential of Diazinon-Degrading Serratia Marcescens to Remove Other Organophosphorus Pesticides from Soils. *J. Environ. Manage.* **2013**, *117*, 7−16.
(11) Wei, W.; Du, J.; Li, J.; Yan, M.; Zhu, Q.; Jin, X.; Zhu, X.; Hu, Z.; Tang, Y.; Lu, Y. Construction of Robust Enzyme Nanocapsules for Effective Organophosphate Decontamination, Detoxification, and Protection. *Adv. Mater.* **2013**, *25*, 2212−2218.
(12) Anwar, S.; Liaquat, F.; Khan, Q. M.; Khalid, Z. M.; Iqbal, S. Biodegradation of Chlorpyrifos and its Hydrolysis Product 3,5,6-trichloro-2-pyridinol by Bacillus Pumilus Strain C2A1. *J. Hazard. Mater.* **2009**, *168*, 400−405.
(13) Hossaini, H.; Moussavi, G.; Farrokhi, M. The Investigation of the LED-Activated FeFNS-TiO_2 Nanocatalyst for Photocatalytic Degradation and Mineralization of Organophosphate Pesticides in Water. *Water Res.* **2014**, *59*, 130−144.
(14) Negishi, N.; Sano, T.; Hirakawa, T.; Koiwa, F.; Chawengkijwanich, C.; Pimpha, N.; Echavia, G.-R. M. Photocatalytic Detoxification of Aqueous Organophosphorus by TiO_2 Immobilized Silica Gel. *Appl. Catal., B* **2012**, *128*, 105−118.
(15) Echavia, G. R. M.; Matzusawa, F.; Negishi, N. Photocatalytic Degradation of Organophosphate and Phosphonoglycine Pesticides using TiO_2 Immobilized on Silica Gel. *Chemosphere* **2009**, *76*, 595−600.
(16) Li, J.-R.; Kuppler, R. J.; Zhou, H.-C. Selective Gas Adsorption and Separation in Metal-Organic Frameworks. *Chem. Soc. Rev.* **2009**, *38*, 1477−1504.
(17) Roberts, J. M.; Fini, B. M.; Sarjeant, A. A.; Farha, O. K.; Hupp, J. T.; Scheidt, K. A. Urea Metal-Organic Frameworks as Effective and Size-selective Hydrogen-Bond Catalysts. *J. Am. Chem. Soc.* **2012**, *134*, 3334−3337.
(18) McDonald, T. M.; Lee, W. R.; Mason, J. A.; Wiers, B. M.; Hong, C. S.; Long, J. R. Capture of Carbon Dioxide from Air and Flue Gas in the Alkylamine-Appended Metal-Organic Framework mmen-Mg_2(dobpdc). *J. Am. Chem. Soc.* **2012**, *134*, 7056−7065.
(19) Gupta, V. K.; Gupta, B.; Rastogi, A.; Agarwal, S.; Nayak, A. A Comparative Investigation on Adsorption Performances of Mesoporous Activated Carbon Prepared from Waste Rubber Tire and Activated Carbon for a Hazardous Azo Dye-Acid Blue 113. *J. Hazard. Mater.* **2011**, *186*, 891−901.
(20) Gupta, V. K.; Gupta, B.; Rastogi, A.; Agarwal, S.; Nayak, A. Pesticides Removal from Waste Water by Activated Carbon Prepared from Waste Rubber Tire. *Water Res.* **2011**, *45*, 4047−4055.
(21) Shukla, P. R.; Wang, S.; Sun, H.; Ang, H. M.; Tadé, M. Activated Carbon Supported Cobalt Catalysts for Advanced Oxidation of Organic Contaminants in Aqueous Solution. *Appl. Catal., B* **2010**, *100*, 529−534.
(22) Yen, C.-W.; Lin, M.-L.; Wang, A.; Chen, S.-A.; Chen, J.-M.; Mou, C.-Y. CO Oxidation Catalyzed by Au−Ag Bimetallic Nanoparticles Supported in Mesoporous Silica. *J. Phys. Chem. C* **2009**, *113*, 17831−17839.
(23) Belmabkhout, Y.; Sayari, A. Effect of Pore Expansion and Amine Functionalization of Mesoporous Silica on CO_2 Adsorption over a Wide Range of Conditions. *Adsorption* **2009**, *15*, 128−138.
(24) Fan, J.; Yu, C.; Gao, F.; Lei, J.; Tian, B.; Wang, L.; Luo, Q.; Tu, B.; Zhou, W.; Zhao, D. Cubic Mesoporous Silica with Large Controllable Entrance Sizes and Advanced Adsorption Properties. *Angew. Chem.* **2003**, *115*, 3254−3258.
(25) Yaghi, O. M.; O'Keeffe, M.; Ockwig, N. W.; Chae, H. K.; Eddaoudi, M.; Kim, J. Reticular Synthesis and the Design of New Materials. *Nature* **2003**, *423*, 705−714.
(26) Kitagawa, S.; Kitaura, R.; Noro, S. Functional Porous Coordination Polymers. *Angew. Chem., Int. Ed.* **2004**, *43*, 2334−2375.
(27) Férey, G. Hybrid Porous Solids: Past, Present, Future. *Chem. Soc. Rev.* **2008**, *37*, 191−214.
(28) Jiang, J.-Q.; Yang, C.-X.; Yan, X.-P. Zeolitic Imidazolate Framework-8 for Fast Adsorption and Removal of Benzotriazoles from Aqueous Solution. *ACS Appl. Mater. Interfaces* **2013**, *5*, 9837−9842.
(29) Li, S.-L.; Lan, Y.-Q.; Sakurai, H.; Xu, Q. Unusual Regenerable Porous Metal−Organic Framework Based on a New Triple Helical Molecular Necklace for Separating Organosulfur Compounds. *Chem.—Eur. J.* **2012**, *18*, 16302−16309.
(30) Cychosz, K. A.; Wong-Foy, A. G.; Matzger, A. J. Liquid Phase Adsorption by Microporous Coordination Polymers: Removal of Organosulfur Compounds. *J. Am. Chem. Soc.* **2008**, *130*, 6938−6939.
(31) Haque, E.; Lo, V.; Minett, A. I.; Harris, A. T.; Church, T. L. Dichotomous Adsorption Behaviour of Dyes on an Amino-Functionalised Metal-Organic Framework, Amino-MIL-101(Al). *J. Mater. Chem. A* **2014**, *2*, 193−203.
(32) Haque, E.; Jun, J. W.; Jhung, S. H. Adsorptive Removal of Methyl Orange and Methylene Blue from Aqueous Solution with a Metal-Organic Framework Material, Iron Terephthalate (MOF-235). *J. Hazard. Mater.* **2011**, *185*, 507−511.
(33) Khan, N. A.; Jung, B. K.; Hasan, Z.; Jhung, S. H. Adsorption and Removal of Phthalic Acid and Diethyl Phthalate from Water with Zeolitic Imidazolate and Metal−Organic Frameworks. *J. Hazard. Mater.* **2014**, *282*, 194−200.
(34) Moreira, M. A.; Santos, J. C.; Ferreira, A. F. P.; Loureiro, J. M.; Ragon, F.; Horcajada, P.; Shim, K.-E.; Hwang, Y.-K.; Lee, U. H.; Chang, J.-S.; Serre, C.; Rodrigues, A. E. Reverse Shape Selectivity in the Liquid-phase Adsorption of Xylene Isomers in Zirconium Terephthalate MOF UiO-66. *Langmuir* **2012**, *28*, 5715−5723.
(35) El Osta, R.; Carlin-Sinclair, A.; Guillou, N.; Walton, R. I.; Vermoortele, F.; Maes, M.; De Vos, D.; Millange, F. Liquid-phase Adsorption and Separation of Xylene Isomers by the Flexible Porous Metal−Organic Framework MIL-53(Fe). *Chem. Mater.* **2012**, *24*, 2781−2791.
(36) Vermoortele, F.; Maes, M.; Moghadam, P. Z.; Lennox, M. J.; Ragon, F.; Boulhout, M.; Biswas, S.; Laurier, K. G. M.; Beurroies, I.; Denoyel, R.; Roeffaers, M.; Stock, N.; Düren, T.; Serre, C.; De Vos, D. E. p-Xylene-Selective Metal−Organic Frameworks: A Case of Topology-Directed Selectivity. *J. Am. Chem. Soc.* **2011**, *133*, 18526−18529.
(37) Khan, N. A.; Jhung, S. H. Remarkable Adsorption Capacity of $CuCl_2$-Loaded Porous Vanadium Benzenedicarboxylate for Benzothiophene. *Angew. Chem.* **2012**, *124*, 1224−1227.
(38) Liu, G.; Lin, Y. Electrochemical Sensor for Organophosphate Pesticides and Nerve Agents using Zirconia Nanoparticles as Selective Sorbents. *Anal. Chem.* **2005**, *77*, 5894−5901.
(39) Zhu, X.; Gu, J.; Wang, Y.; Li, B.; Li, Y.; Zhao, W.; Shi, J. Inherent Anchorage in UiO-66 Nanoparticles for Efficient Capture of Alendronate and its Mediated Release. *Chem. Commun.* **2014**, *50*, 8779−8782.
(40) Nguyen, H. G. T.; Schweitzer, N. M.; Chang, C.-Y.; Drake, T. L.; So, M. C.; Stair, P. C.; Farha, O. K.; Hupp, J. T.; Nguyen, S. T. Vanadium-Node-Functionalized UiO-66: A Thermally Stable MOF-Supported Catalyst for the Gas-Phase Oxidative Dehydrogenation of Cyclohexene. *ACS Catal.* **2014**, *4*, 2496−2500.
(41) Balci, B.; Oturan, M. A.; Oturan, N.; Sirés, I. Decontamination of Aqueous Glyphosate, (Aminomethyl)phosphonic Acid, and Glufosinate Solutions by Electro-Fenton-like Process with Mn^{2+} as the Catalyst. *J. Agric. Food. Chem.* **2009**, *57*, 4888−4894.
(42) Duke, S. O.; Powles, S. B. Glyphosate: A Once-in-a-Century Herbicide. *Pest Manage. Sci.* **2008**, *64*, 319−325.

DOI: 10.1021/am5059074
ACS Appl. Mater. Interfaces 2015, 7, 223−231

(43) Khenifi, A.; Derriche, Z.; Mousty, C.; Prévot, V.; Forano, C. Adsorption of Glyphosate and Glufosinate by Ni_2AlNO_3 Layered Double Hydroxide. *Appl. Clay Sci.* **2010**, *47*, 362−371.
(44) Cavka, J. H.; Jakobsen, S.; Olsbye, U.; Guillou, N.; Lamberti, C.; Bordiga, S.; Lillerud, K. P. A New Zirconium Inorganic Building Brick Forming Metal Organic Frameworks with Exceptional Stability. *J. Am. Chem. Soc.* **2008**, *130*, 13850−13851.
(45) Vermoortele, F.; Bueken, B.; Le Bars, G.; Van de Voorde, B.; Vandichel, M.; Houthoofd, K.; Vimont, A.; Daturi, M.; Waroquier, M.; Van Speybroeck, V.; Kirschhock, C.; De Vos, D. E. Synthesis Modulation as a Tool to Increase the Catalytic Activity of Metal-Organic Frameworks: The Unique Case of UiO-66 (Zr). *J. Am. Chem. Soc.* **2013**, *135*, 11465−11468.
(46) Katz, M. J.; Brown, Z. J.; Colon, Y. J.; Siu, P. W.; Scheidt, K. A.; Snurr, R. Q.; Hupp, J. T.; Farha, O. K. A Facile Synthesis of UiO-66, UiO-67 and their Derivatives. *Chem. Commun.* **2013**, *49*, 9449−9451.
(47) Barrett, S. M.; Wang, C.; Lin, W. Oxygen Sensing via Phosphorescence Quenching of Doped Metal-Organic Frameworks. *J. Mater. Chem.* **2012**, *22*, 10329−10334.
(48) Wu, H.; Chua, Y. S.; Krungleviciute, V.; Tyagi, M.; Chen, P.; Yildirim, T.; Zhou, W. Unusual and Highly Tunable Missing-Linker Defects in Zirconium Metal−Organic Framework UiO-66 and Their Important Effects on Gas Adsorption. *J. Am. Chem. Soc.* **2013**, *135*, 10525−10532.
(49) Schaate, A.; Roy, P.; Godt, A.; Lippke, J.; Waltz, F.; Wiebcke, M.; Behrens, P. Modulated Synthesis of Zr-based Metal-Organic Frameworks: From Nano to Single Crystals. *Chem.—Eur. J.* **2011**, *17*, 6643−6651.
(50) Ho, Y.-S.; McKay, G. Pseudo-Second Order Model for Sorption Processes. *Process Biochem.* **1999**, *34*, 451−465.
(51) Ho, Y.-S.; McKay, G. The Kinetics of Sorption of Divalent Metal Ions onto Sphagnum Moss Peat. *Water Res.* **2000**, *34*, 735−742.
(52) Ghorai, S.; Sarkar, A.; Raoufi, M.; Panda, A. B.; Schönherr, H.; Pal, S. Enhanced Removal of Methylene Blue and Methyl Violet Dyes from Aqueous Solution using a Nanocomposite of Hydrolyzed Polyacrylamide Grafted Xanthan Gum and Incorporated Nanosilica. *ACS Appl. Mater. Interfaces* **2014**, *6*, 4766−4777.
(53) Hameed, B. H.; Salman, J. M.; Ahmad, A. L. Adsorption Isotherm and Kinetic Modeling of 2,4-D Pesticide on Activated Carbon Derived from Date Stones. *J. Hazard. Mater.* **2009**, *163*, 121−126.
(54) Slowing, I. I.; Trewyn, B. G.; Lin, V. S.-Y. Mesoporous Silica Nanoparticles for Intracellular Delivery of Membrane-Impermeable Proteins. *J. Am. Chem. Soc.* **2007**, *129*, 8845−8849.
(55) Jonsson, C. M.; Persson, P.; Sjöberg, S.; Loring, J. S. Adsorption of Glyphosate on Goethite (α-FeOOH): Surface Complexation Modeling Combining Spectroscopic and Adsorption Data. *Environ. Sci. Technol.* **2008**, *42*, 2464−2469.
(56) Khoury, G. A.; Gehris, T. C.; Tribe, L.; Torres Sánchez, R. M.; dos Santos Afonso, M. Glyphosate Adsorption on Montmorillonite: An Experimental and Theoretical Study of Surface Complexes. *Appl. Clay Sci.* **2010**, *50*, 167−175.
(57) Hu, Y. S.; Zhao, Y. Q.; Sorohan, B. Removal of Glyphosate from Aqueous Environment by Adsorption using Water Industrial Residual. *Desalination* **2011**, *271*, 150−156.
(58) Milojević-Rakić, M.; Janošević, A.; Krstić, J.; Nedić Vasiljević, B.; Dondur, V.; Ćirić-Marjanović, G. Polyaniline and its Composites with Zeolite ZSM-5 for Efficient Removal of Glyphosate from Aqueous Solution. *Microporous Mesoporous Mater.* **2013**, *180*, 141−155.
(59) Zheng, Y.-M.; Yu, L.; Wu, D.; Paul Chen, J. Removal of Arsenite from Aqueous Solution by a Zirconia Nanoparticle. *Chem. Eng. J.* **2012**, *188*, 15−22.
(60) Li, J.; Zhang, S.; Chen, C.; Zhao, G.; Yang, X.; Li, J.; Wang, X. Removal of Cu(II) and Fulvic Acid by Graphene Oxide Nanosheets Decorated with Fe_3O_4 Nanoparticles. *ACS Appl. Mater. Interfaces* **2012**, *4*, 4991−5000.
(61) Hayes, K. F.; Papelis, C.; Leckie, J. O. Modeling Ionic Strength Effects on Anion Adsorption at Hydrous Oxide/Solution Interfaces. *J. Colloid Interface Sci.* **1988**, *125*, 717−726.
(62) Gu, J.; Huang, M.; Liu, J.; Li, Y.; Zhao, W.; Shi, J. Calcium Doped Mesoporous Silica Nanoparticles as Efficient Alendronate Delivery vehicles. *New J. Chem.* **2012**, *36*, 1717−1720.
(63) Daou, T. J.; Begin-Colin, S.; Grenèche, J. M.; Thomas, F.; Derory, A.; Bernhardt, P.; Legaré, P.; Pourroy, G. Phosphate Adsorption Properties of Magnetite-based Nanoparticles. *Chem. Mater.* **2007**, *19*, 4494−4505.
(64) Joo, J.; Yu, T.; Kim, Y. W.; Park, H. M.; Wu, F.; Zhang, J. Z.; Hyeon, T. Multigram Scale Synthesis and Characterization of Monodisperse Tetragonal Zirconia Nanocrystals. *J. Am. Chem. Soc.* **2003**, *125*, 6553−6557.
(65) Wu, K. C.-W.; Yamauchi, Y.; Hong, C.-Y.; Yang, Y.-H.; Liang, Y.-H.; Funatsu, T.; Tsunoda, M. Biocompatible, Surface Functionalized Mesoporous Titania Nanoparticles for Intracellular Imaging and Anticancer Drug Delivery. *Chem. Commun.* **2011**, *47*, 5232−5234.
(66) Mondloch, J. E.; Bury, W.; Fairen-Jimenez, D.; Kwon, S.; DeMarco, E. J.; Weston, M. H.; Sarjeant, A. A.; Nguyen, S. T.; Stair, P. C.; Snurr, R. Q.; Farha, O. K.; Hupp, J. T. Vapor-Phase Metalation by Atomic Layer Deposition in a Metal−Organic Framework. *J. Am. Chem. Soc.* **2013**, *135*, 10294−10297.
(67) Valenzano, L.; Civalleri, B.; Chavan, S.; Bordiga, S.; Nilsen, M. H.; Jakobsen, S.; Lillerud, K. P.; Lamberti, C. Disclosing the Complex Structure of UiO-66 Metal Organic Framework: A Synergic Combination of Experiment and Theory. *Chem. Mater.* **2011**, *23*, 1700−1718.
(68) Larabi, C.; Quadrelli, E. A. Titration of Zr(μ_3-OH) Hydroxy Groups at the Cornerstones of Bulk MOF UiO-67, $[Zr_6O_4(OH)_4(biphenyldicarboxylate)_6]$, and Their Reaction with $[AuMe(PMe_3)]$. *Eur. J. Inorg. Chem.* **2012**, *2012*, 3014−3022.

DOI: 10.1021/am5059074
ACS Appl. Mater. Interfaces 2015, 7, 223−231